

Electric dipole response of ^{208}Pb from proton inelastic scattering: constraints on neutron skin thickness and symmetry energy

A. Tamii¹, P. von Neumann-Cosel², and I. Poltoratska²

¹ Research Center for Nuclear Physics, 10-1 Mihogaoka, Ibaraki 567-0047, Japan

² Institut für Kernphysik, Technische Universität Darmstadt, D-64289 Darmstadt, Germany

Received: date / Revised version: date

Abstract. The electric dipole ($E1$) response of ^{208}Pb has been precisely determined by measuring Coulomb excitation induced by proton scattering at very forward angles. The electric dipole polarizability, defined as inverse energy-weighted sum rule of the $E1$ strength, has been extracted as $\alpha_D = 20.1 \pm 0.6 \text{ fm}^3$. The data can be used to constrain the neutron skin thickness of ^{208}Pb to $\Delta r_{np} = 0.165 \pm (0.009)_{\text{expt}} \pm (0.013)_{\text{theor}} \pm (0.021)_{\text{est}} \text{ fm}$, where the subscript “expt” refers to the experimental uncertainty, “theor” to the theoretical confidence band and “est” to the uncertainty associated with the estimation of the symmetry energy at the saturation density. In addition, a constraint band has been extracted in the plane of the symmetry energy (J) and its slope parameter (L) at the saturation density.

PACS. 25.40.Ep Inelastic proton scattering – 27.80.+w $190 \leq A \leq 219$ – 24.30.Cz Giant resonances – 21.65.Ef Symmetry energy

1 Introduction

The nuclear equation of state (EOS) defines the bulk properties of nuclear matter from atomic nuclei to neutron stars. Determination of the nuclear EOS is one of the fundamental goals of nuclear physics. Since nuclear matter is composed of two kinds of particles, *i.e.* neutrons and protons, the EOS contains a term – the symmetry energy – which depends on the density asymmetry between neutrons and protons. Determination of the symmetry energy term currently draws much attention both theoretically and experimentally, as illustrated by this special issue. An accurate determination of the symmetry energy allows precise predictions of properties of exotic nuclei with large differences between proton and neutron numbers. The symmetry energy is furthermore a basic input for calculations of heavy-ion collision processes, where isospin-asymmetric matter is produced and leads to density-dependent reactions. In astrophysics, the symmetry energy is relevant to the properties of neutron stars, such as mass, radius and internal structure, the supernova-explosion process, neutron star cooling, and other dynamical processes related to neutron rich matter.

The nuclear EOS can be studied in laboratory by measuring data on nuclear ground and excited states and constructing theoretical models which attempt to describe them. In this article, we report on a precise determination of the electric dipole response of ^{208}Pb by measuring relativistic Coulomb excitation induced by proton inelastic scattering at very forward angles. The dipole polariz-

ability, defined as the inverse energy-weighted sum rule of the electric dipole response, is closely related to the neutron skin thickness and to the density dependence of the symmetry energy.

2 Relation between symmetry energy, neutron skin thickness and dipole polarizability

The EOS of cold nuclear matter can be approximately written as a sum of the energy per nucleon of symmetric matter and an asymmetry term [1]

$$E(\rho, \delta) = E(\rho, \delta = 0) + S(\rho)\delta^2 + O(\delta^4), \quad (1)$$

where the nucleon density (ρ) and the asymmetry parameter (δ) are defined by the neutron (ρ_n) and proton (ρ_p) density as

$$\rho \equiv \rho_n + \rho_p, \quad (2)$$

$$\delta \equiv \frac{\rho_n - \rho_p}{\rho_n + \rho_p}. \quad (3)$$

The symmetry energy factor $S(\rho)$ in Eq. (1) can be expanded around the saturation density $\rho_0 \sim 0.16 \text{ fm}^{-3}$ as

$$S(\rho) = J + \frac{L}{3\rho_0}(\rho - \rho_0) + \frac{K_{\text{sym}}}{18\rho_0^2}(\rho - \rho_0)^2 + \dots \quad (4)$$

Here, L is the slope parameter at density ρ_0 . It governs the pressure from the symmetry energy in pure neutron

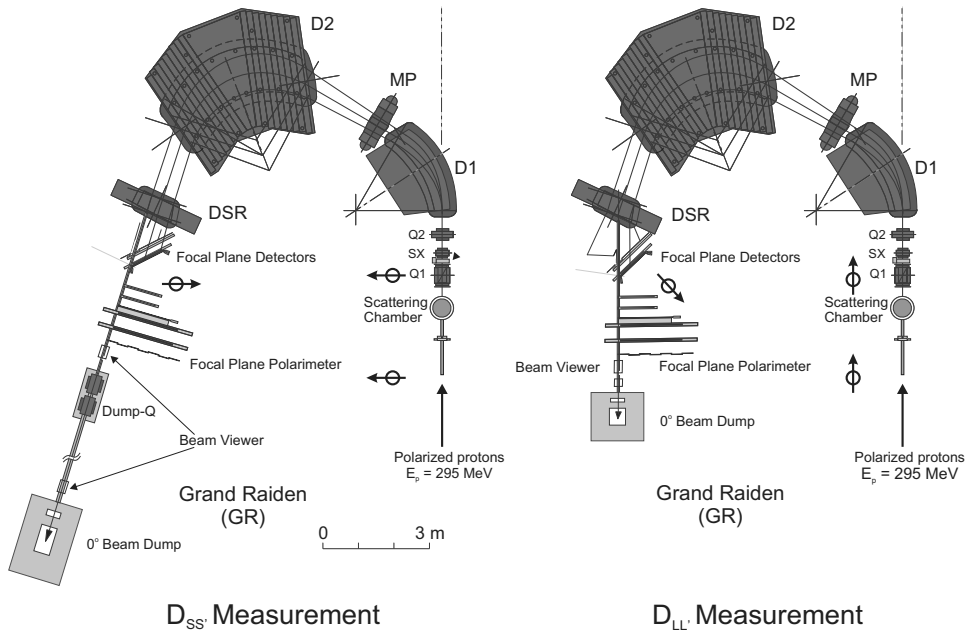


Fig. 1. Experimental setup of the Grand Raiden spectrometer at zero degree for the measurement of the $D_{SS'}$ (left) and $D_{LL'}$ (right) polarization transfer coefficients in inelastic proton scattering off ^{208}Pb at $E_0 = 295$ MeV. See text for details.

matter and the baryonic pressure in neutron stars [2], and its value is approximately proportional to the fourth power of the neutron star radius [3].

Linear correlations between the slope parameter and the neutron skin thickness of ^{208}Pb are predicted by self-consistent mean field model calculations with various sets of interaction parameters [4,5]. Here, the neutron skin thickness Δr_{np} is defined as the difference of the root-mean-square radii of neutrons and protons. Thus, experimental data on the neutron skin thickness may provide constraints on the slope parameter.

Parity-violating asymmetry measurements of electron elastic scattering (PREX experiment) at Jefferson Laboratory [6] are the most model-independent way to determine the neutron skin thickness of ^{208}Pb . The electro-weak interaction is used to probe the form factor of the neutron density distribution. However the uncertainty of the latest result, $\Delta r_{np} = 0.302 \pm 0.175 \pm 0.026 \pm 0.005$ fm [7], is too large to impact on the allowed range of the slope parameter. An improved measurement with better statistics is highly desired.

Reinhard and Nazarewicz reported a strong correlation between the dipole polarizability of ^{208}Pb and its neutron skin thickness in the framework of a self-consistent mean field calculation based on the energy-density functional method with the SV_{min} Skyrme interaction [8]. The dipole polarizability α_D can be expressed as the inverse energy-weighted sum-rule of the electric dipole ($E1$) reduced transition probability $B(E1)$

$$\alpha_D = \frac{\hbar c}{2\pi^2} \int \frac{\sigma_{\text{abs}}}{\omega^2} d\omega = \frac{8\pi}{9} \int \frac{S_{E1}(\omega)}{\omega} d\omega, \quad (5)$$

where ω stands for the excitation energy, σ_{abs} for the photo-absorption cross section, and $S_{E1}(\omega) = dB(E1)/d\omega$

for the $B(E1)$ strength per unit excitation energy. The dipole polarizability can be experimentally determined by measuring the $B(E1)$ distribution as a function of the excitation energy. We have used proton inelastic scattering at very forward angles to study the $B(E1)$ distribution of ^{208}Pb by relativistic Coulomb excitation.

3 Experimental Method

The experiment has been performed at the Research Center for Nuclear Physics (RCNP), Osaka University. Details of the experimental method can be found in Ref. [9] and details for the ^{208}Pb experiment in Refs. [10, 11]. A polarized proton beam has been accelerated to 295 MeV with a beam intensity of 2-10 nA and a polarization degree of about 0.7. An isotopically enriched ^{208}Pb foil with a thickness of 5.2 mg/cm^2 has been used as a target. An energy resolution of 30 keV (FWHM) was achieved by dispersion matching techniques. The experimental setup is shown in Fig. 1 for two different polarization transfer measurements. The primary beam passing through the target was transported into the *Grand Raiden* spectrometer [12], extracted at the focal plane, and stopped in the beam dump. The sideways-to-sideways polarization transfer $D_{SS'}$ (l.h.s. of Fig. 1) was measured with a sideways polarized beam and the standard focal plane without use of the dipole spin-rotation (DSR) magnet. The longitudinal-to-longitudinal polarization transfer $D_{LL'}$ (r.h.s. of Fig. 1) was measured with a longitudinally polarized beam and rotation of the scattered protons by 18° utilizing the DSR magnet. Polarization transfer coefficients were measured in an angular range $0^\circ - 2.5^\circ$. Differential cross sections were measured for angles between 0 and 10 degrees. The

excitation energy range covered by the momentum acceptance of the spectrometer was about 5 – 25 MeV.

4 Experimental results

The upper panel of Fig. 2 shows the double differential cross section of the $^{208}\text{Pb}(p,p')$ reaction with the spectrometer set at 0° and covering an angular range up to 2.5° . The giant dipole resonance (GDR) is clearly visible as bump structure centered at about 13 MeV with fine structures on the lower-energy tail. Discrete transitions were observed below the neutron separation energy ($S_n=7.368$ MeV).

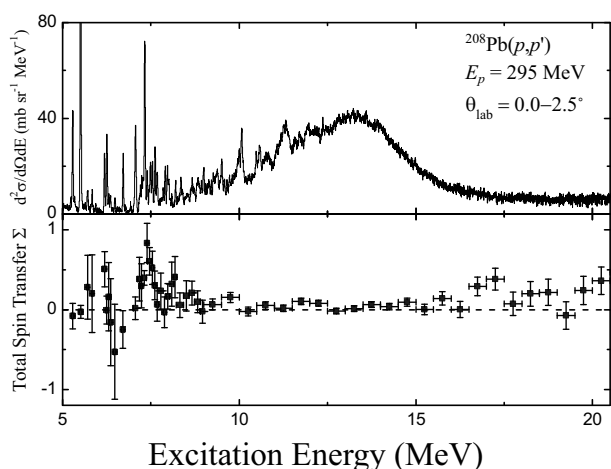


Fig. 2. (upper panel) Double differential cross sections and (lower panel) total spin transfer of the $^{208}\text{Pb}(p,p')$ reaction at $E_p=295$ MeV and at $0-2.5$ degrees.

As demonstrated in Fig. 3, there is a one-to-one correspondence with $E1$ transitions observed in nuclear resonance fluorescence (NRF) measurements [13, 14, 15, 16]. For each low-lying discrete transition, the $B(E1)$ strength has been extracted from the (p,p') cross sections in the angular range $0^\circ - 0.94^\circ$ assuming that it arises purely from Coulomb excitation. The extracted $B(E1)$ values agree very well with the NRF data below S_n [13, 14, 15, 16]. Above S_n more strength than previously known has been observed [11].

Since the experimental kinematics also favor excitation of the spin- $M1$ resonance, a decomposition of $E1$ and $M1$ cross sections is necessary for an extraction of the $E1$ strength in the continuum region. This has been achieved with two independent methods. The first method utilizes polarization transfer data. One can define the total spin transfer Σ

$$\Sigma \equiv \frac{3 - (D_{SS'} + D_{NN'} + D_{LL'})}{4}, \quad (6)$$

where $D_{SS'}$, $D_{NN'}$ and $D_{LL'}$ are the sideway, normal and longitudinal spin transfer coefficients, respectively [17].

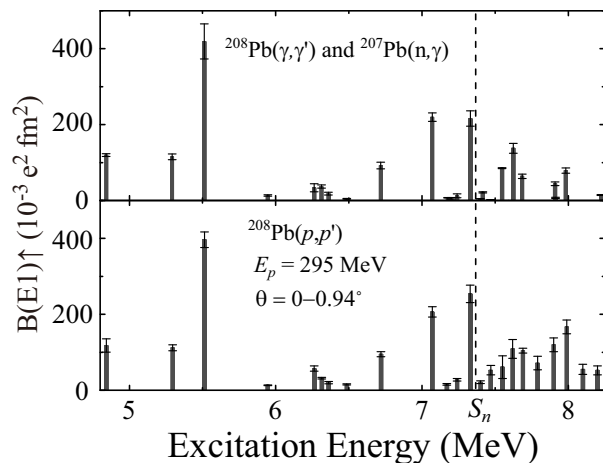


Fig. 3. Electric dipole reduced transition probability $B(E1)$ of low-lying discrete states determined by (upper panel) real-photon measurements [13, 14, 15, 16] and (lower panel) the (p,p') experiment.

The total spin transfer Σ becomes unity for spin- $M1$ and other spin-flip excitations by the nuclear interaction and zero for (Coulomb-excited) $E1$ and other non-spin-flip excitations. Relation (6) can be derived at zero degrees from parity conservation [18] and thus holds model-independently. Note that $D_{SS'} = D_{NN'}$ at zero degrees from rotational symmetry, and therefore only two polarization transfer coefficients need to be measured. The resulting total spin transfer for ^{208}Pb is plotted in the lower panel of Fig. 2. The GDR bump region is dominantly composed of $E1$ strength. A concentration of spin- $M1$ strength is observed in the 7 – 8 MeV region consistent with polarized real-photon measurements [15, 19].

The second method is a multipole-decomposition analysis (MDA) utilizing the angular distributions of the cross sections in each excitation energy bin to decompose contributions from different multipolarities. Angular distribution shapes for each multipolarity were calculated in the distorted wave impulse approximation (DWIA) with the code DWBA07 [20] and the effective interaction of Franey and Love [21]. RPA amplitudes and single-particle wave functions were taken from quasi-particle phonon model (QPM) calculations [13]. For each energy bin, the contributions of different multipolarities were determined by a least-square fit reproducing the experimental angular distribution. The results of the two methods agree to each other within error bars [10]. The $E1$ photo-absorption cross section in the GDR region extracted by the MDA is shown in Fig. 4 as red circles. The result is consistent with (γ, xn) [22] (black histogram) and tagged-photon [23] (green squares) measurements.

The overall $B(E1)$ distribution determined by the (p,p') measurement is shown in Fig. 5. The bump centered at ~ 13 MeV corresponds to the GDR and the strength concentration around 7–9 MeV corresponds to the pygmy dipole resonance (PDR). A complete $B(E1)$ strength distribution of ^{208}Pb has been determined from 5 to 20 MeV

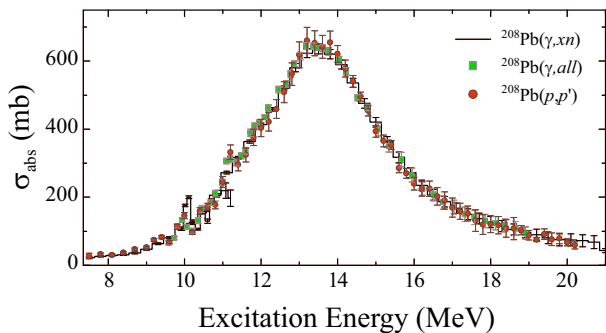


Fig. 4. Comparison of photo-absorption cross sections determined by (p, p') (red circles), (γ, xn) [22] (histogram) and tagged gamma-absorption [23] (green squares) experiments in the GDR region of ^{208}Pb .

which fully covers the PDR and GDR regions, as well as region just above neutron separation energy, where all previous experiments had limited sensitivity.

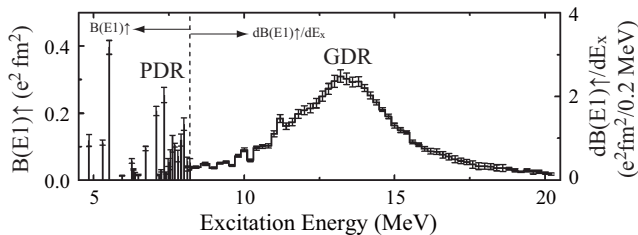


Fig. 5. Total $B(E1)$ strength distribution of ^{208}Pb deduced from the present work. The bump centered at ~ 13 MeV corresponds to the giant dipole resonance, and the strength concentration at around 7-9 MeV to the pygmy dipole resonance.

5 Dipole polarizability and neutron skin thickness in ^{208}Pb

The obtained $B(E1)$ strength distribution is integrated with the aid of Eq. (5) and yields a dipole polarizability $\alpha_D = 18.9 \pm 1.3 \text{ fm}^3$ up to 20 MeV. By taking the average over the independent data sets and by including the gamma absorption data above 20 MeV [23], the dipole polarizability of ^{208}Pb up to 130 MeV is determined as $\alpha_D = 20.1 \pm 0.6 \text{ fm}^3$.

Reinhard and Nazarewicz have shown [8] that in mean-field models, for variations of the interaction within reasonable limits there is a strict correlation between the predictions for the dipole polarizability and neutron skin thickness of ^{208}Pb . With the particular interaction of Ref. [8] one can derive from the above experimental result for α_D a value $\Delta r_{np} = 0.156_{-0.021}^{+0.025} \text{ fm}$ [10]. Piekarewicz *et al.* [5] have studied this correlation for a variety of non-relativistic and relativistic density functionals (EDFs).

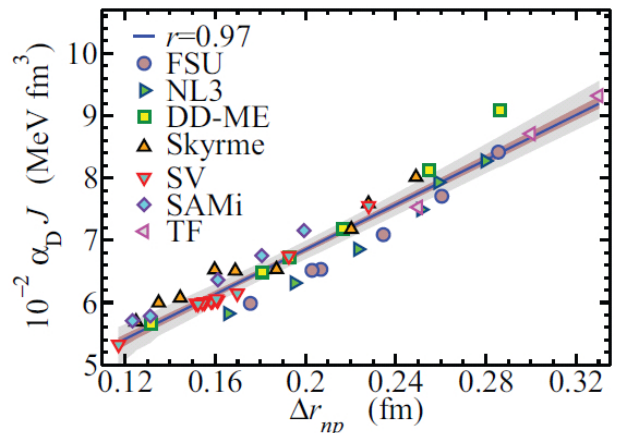


Fig. 6. Correlation between the dipole polarizability α_D times J and the neutron skin thickness Δr_{np} in ^{208}Pb for various mean-field models. Figure reprinted with permission from X. Roca-Maza *et al.* [25]. Copyright (2013) by the American Physical Society.

However, absolute values, while indicating an overall approximately linear correlation, exhibit more scattering upon a detailed look. If averaged over the set of theoretical results falling into the experimental uncertainty of α_D , one obtains a value for the neutron skin thickness in ^{208}Pb of $0.168 \pm 0.022 \text{ fm}$ [5]. Roca-Maza *et al.* [25] have further investigated the correlation. They have found that $\alpha_D J$, instead of α_D , has much stronger correlation with Δr_{np} (see Fig. 6) and the correlation is naturally explained by the macroscopic droplet model. The value of the neutron skin thickness of ^{208}Pb as a function of J is, by using the experimental value of α_D

$$\Delta r_{np} = -0.157 \pm (0.002)_{\text{theor}} + [1.04 \pm (0.03)_{\text{expt}} \pm (0.04)_{\text{theor}}] \times 10^{-2} J, \quad (7)$$

where Δr_{np} is expressed in fm and J in MeV. The “expt” uncertainty refers to the propagation of the experimental uncertainty of α_D , whereas the “theor” uncertainties are associated with the confidence bands from the theoretical linear fit. Adopting $J = [31 \pm (2)_{\text{est}}] \text{ MeV}$ as a realistic range of values for the symmetry energy [1,26], they extracted the constraint on the neutron skin thickness of ^{208}Pb as [25]

$$\Delta r_{np} = 0.165 \pm (0.009)_{\text{expt}} \pm (0.013)_{\text{theor}} \pm (0.021)_{\text{est}} \text{ fm}, \quad (8)$$

where “est” uncertainty is associated with the estimates on J .

This result is compared with other experimental work in Fig. 7. The inner error bar of the dipole polarizability analysis refers to the experimental uncertainty (0.009 fm) and the outer error bar to the quadratic sum of all the uncertainties (0.026 fm). As pointed out above, the statistics of the PREX experiment are presently insufficient to provide relevant boundaries on the neutron skin thickness [7]. Antiprotonic atom annihilation and shifts of X rays have been used to derive the neutron density

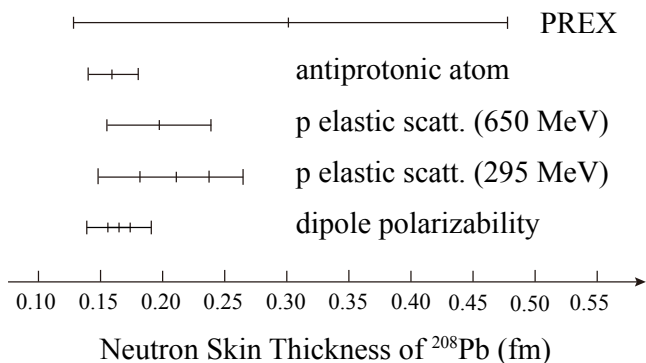


Fig. 7. The neutron skin thickness of ^{208}Pb measured by parity-violating electron scattering (PREX) [6,7], analysis of the X-ray detection data of anti-protonic atoms [27], proton elastic scattering at 650 MeV [28] and 295 MeV [29], and the dipole polarizability (this work) [10,25].

of ^{208}Pb , and combined with the charge density distribution the neutron skin thickness [24,27]. Another method is based on extracting the matter radius from elastic proton scattering. Two results obtained at 650 MeV [28] and 295 MeV [29] are currently available. All results agree within error bars and limit the range of the neutron skin thickness to $\sim 0.15 - 0.20$ fm. Recent calculations of neutron matter and neutron star properties in the framework of chiral effective field theory suggest $\Delta r_{np} = 0.17 \pm 0.03$ fm [30]. The predictions are sensitive to three-nucleon forces, which may be further constrained by the present results.

6 Constraints on the symmetry energy

Mean-field models predict an approximately linear relation between the neutron skin thickness of ^{208}Pb and the slope parameter L of the symmetry energy [4,32]. Thus one can also expect a linear relation between $\alpha_D J$ and L . Actually Roca-Maza *et al.* [25] have shown a strong correlation between $\alpha_D J$ and L . [25] They have extracted the relation by using the dipole polarizability data as

$$L = -146 \pm (1)_{\text{theor}} + [6.11 \pm (0.18)_{\text{expt}} \pm (0.26)_{\text{theor}}] J, \quad (9)$$

and by adopting $J = [31 \pm (2)_{\text{est}}]$ MeV

$$L = 43 \pm (6)_{\text{expt}} \pm (8)_{\text{theor}} \pm (12)_{\text{est}} \text{ MeV}. \quad (10)$$

Since constraints on the symmetry energy parameters J and L are the main concern in this paper, we have extracted a constraint band in the J - L plane from the dipole polarizability data without making assumption on the J value. We have taken the quadratic sum of the 99.9% theoretical confidence level band from the work by Roca-Maza *et al.* [25] and the one-sigma experimental uncertainty of α_D [10]. Within the applicable range of $24 < J < 42$ MeV, the band is placed in between the two curves of $L = -93.5 + 3.22J + 0.0461J^2$

and $L = -182.4 + 7.85J - 0.0266J^2$. If the two-sigma experimental uncertainty of α_D is used, the constraint band is in between $L = -111.0 + 4.43J + 0.0307J^2$ and $L = -172.0 + 7.12J - 0.0189J^2$.

The result is plotted in Fig. 8 for the one-sigma uncertainty in comparison with various constraints from other works. These include heavy ion collisions (HIC), pygmy dipole resonance (PDR), isobaric analog states (IAS), nuclear mass formula with finite range droplet model (FRDM), analysis of neutron star observation data (n-star). For a thorough discussion of these methods and the corresponding references see Ref. [1]. Additionally, constraints from a chiral effective field theory (χ EFT) calculation including $3N$ forces [30] and a quantum Monte-Carlo (QMC) calculation [31] are shown. One finds a point ($L \approx 50$ MeV, $J \approx 32$ MeV) essentially consistent with all approaches except for the study of isobaric analogue states which requires much higher values of L . Indeed, these common values are at the center of the allowed L, J landscape in the first complete $N^3\text{LO}$ calculation of neutron matter within χ EFT [33].

We note that in the paper of Lattimer [34] an anticorrelation between the L and J is deduced from α_D of ^{208}Pb based on a Skyrme-Hartree-Fock approach [35] in contradiction to the present result. The anticorrelation originates from a two step evaluation of the constraint in the J - L plane from α_D by way of Δr_{np} , whereas the present result is more direct.

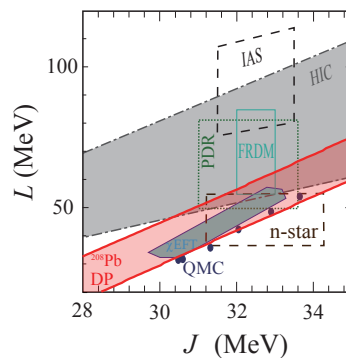


Fig. 8. Constraints on the symmetry energy parameters J and L from various methods. Besides the present work based on the ^{208}Pb dipole polarizability (DP), the results in this figure are taken from Ref. [1] except the ones labeled (χ EFT) from Ref. [30] and QMC (solid circles) from Ref. [31].

7 Summary and outlook

The electric dipole response of ^{208}Pb has been determined up to 20 MeV by proton inelastic scattering measurement at extreme forward angles. Multipole components of the

cross sections have been decomposed by two independent methods: polarization transfer analysis and angular distribution analysis. The dipole polarizability of ^{208}Pb up to 130 MeV was determined as $\alpha_D = 20.1 \pm 0.6 \text{ fm}^3$ by combining the present and other available data. This precise result allows to constrain the neutron skin thickness of ^{208}Pb to $\Delta r_{np} = 0.165 \pm (0.009)_{\text{expt}} \pm (0.013)_{\text{theor}} \pm (0.021)_{\text{est}}$ fm. A constraint band has been extracted for the symmetry energy and its slope parameter at the saturation density utilizing the correlations between $\alpha_D J$ and L obtained by a study of mean-field models in EDF approach. The accuracy already sets important constraints for model parameters of EDFs and predictions of neutron star properties, supernova explosion dynamics, and many other interesting astrophysical phenomena.

In order to further constrain the symmetry energy parameters – or more precisely EDF approaches, from which they can be derived –, dipole polarizability data for other nuclei would be important. A particularly interesting candidate is ^{48}Ca , for which theoretical predictions (especially with Skyrme-type forces) of the neutron skin thickness are more scattered and relatively uncorrelated with that of ^{208}Pb [5]. Proton inelastic scattering data on ^{48}Ca are already measured. Analysis and extraction of the dipole polarizability for ^{48}Ca is in progress as well as for ^{90}Zr [37], ^{96}Mo , ^{120}Sn , $^{144,154}\text{Sm}$.

Beyond the extraction of the dipole polarizability, we note that the experimental data provide information on the PDR strength distribution [11,37], the spin-M1 strength distribution [38,39], fine structure of the GDR and its interpretation in terms of characteristic scales [40], level density of the $E1$ strength using a fluctuation analysis [41,42], and the gamma strength function.

Acknowledgments

This work was performed by the RCNP-E282 collaboration and we thank all coauthors of Refs. [10,11] for their contributions. We are indebted to the RCNP cyclotron accelerator staff and operators for providing an excellent beam. Discussions with W. Nazarewicz, J. Piekarewicz, P.-G. Reinhard, A. Schwenk, and X. Roca-Maza are gratefully acknowledged. This work was supported by JSPS (Grant Nos. 07454051 and 14740154) and DFG (Contracts SFB 634 and NE 679/3-1).

References

1. M.B. Tsang *et al.*, *Phys. Rev. C* **86**, 015803 (2012).
2. C.J. Horowitz, J. Piekarewicz, *Phys. Rev. Lett.* **86**, 5647 (2001).
3. J.M. Lattimer and M. Prakash, *Phys. Rep.* **442**, 109 (2007).
4. X. Roca-Maza, M. Centelles, X. Viñas, M. Warda, *Phys. Rev. Lett.* **106**, 252501 (2011).
5. J. Piekarewicz *et al.*, *Phys. Rev. C* **85**, 041302(R) (2012).
6. S. Abrahamyan *et al.*, *Phys. Rev. Lett.* **108**, 112502 (2012).
7. C.J. Horowitz *et al.*, *Phys. Rev. C* **85**, 032501(R) (2012).
8. P.-G. Reinhard, W. Nazarewicz, *Phys. Rev. C* **81**, 051303(R) (2010).
9. A. Tamii *et al.*, *Nucl. Instrum. Meth. in Phys. Res. Sect. A* **605**, 326 (2009).
10. A. Tamii *et al.*, *Phys. Rev. Lett.* **107**, 062502 (2011).
11. I. Poltoratska, *et al.*, *Phys. Rev. C* **85**, 041304(R) (2012).
12. M. Fujiwara *et al.*, *Nucl. Instrum. Meth. in Phys. Res. Sect. A* **422**, 484 (1999).
13. N. Ryezayeva *et al.*, *Phys. Rev. Lett.* **89**, 272502 (2002).
14. J. Enders *et al.*, *Nucl. Phys. A* **724**, 243 (2003);
15. T. Shizuma *et al.*, *Phys. Rev. C* **78**, 061303(R) (2008).
16. R. Schwengner *et al.*, *Phys. Rev. C* **81**, 054315 (2010).
17. G.G. Ohlsen, *Rep. Prog. Phys.* **35**, 717 (1972).
18. T. Suzuki, *Prog. Theor. Phys.* **103**, 859 (2000).
19. R.M. Laszewski, R. Alarcon, D.S. Dale, S.D. Hoblit, *Phys. Rev. Lett.* **61**, 1710(1988).
20. J. Raynal, computer code *DWBA07*, NEA data bank NEA-1209.
21. M.A. Franey and W.G. Love, *Phys. Rev. C* **31**, 488 (1985).
22. A. Veyssiere *et al.*, *Nucl. Phys. A* **159**, 561 (1970).
23. K.P. Schelhaas *et al.*, *Nucl. Phys. A* **489**, 189 (1988).
24. A. Trzczińska *et al.*, *Phys. Rev. Lett.* **87**, 082501 (2001).
25. X. Roca-Maza, M. Brenna, G. Colò *et al.*, *Phys. Rev. C* **88**, 024316 (2013).
26. J.M. Lattimer and Y. Lim *Astrophys. J.* **771**, 51 (2013).
27. B. Klos *et al.*, *Phys. Rev. C* **76**, 014311 (2007).
28. V.E. Starodubsky and N.M. Hintz, *Phys. Rev. C* **49**, 2118 (1994).
29. J. Zenihiro *et al.*, *Phys. Rev. C* **82**, 044611 (2010).
30. K. Hebeler, J.M. Lattimer, C.J. Pethick, A. Schwenk, *Phys. Rev. Lett.* **105**, 161102 (2010).
31. S. Gandolfi, J. Carlson, S. Reddy, W. Steiner, and R.B. Wiringa *et al.*, arXiv:1307.5815 [nucl-th] (2013); S. Gandolfi, private communication.
32. B.A. Brown, *Phys. Rev. Lett.* **85**, 5296 (2000); S. Typel and B.A. Brown, *Phys. Rev. C* **64**, 027302 (2001).
33. I. Tews, T. Krüger, K. Hebeler, and A. Schwenk, *Phys. Rev. Lett.* **110**, 032504 (2013).
34. J.M. Lattimer, *Annu. Rev. Nucl. Part. Sci.* **62**, 485 (2012).
35. Lie-Wen Chen, Che Ming Ko, Bao-An Li, Jun Xu, *Phys. Rev. C* **82**, 024321 (2010).
36. X. Roca-Maza, private communication.
37. C. Iwamoto *et al.*, *Phys. Rev. Lett.* **108**, 262501 (2012).
38. K. Heyde, P. von Neumann-Cosel, A. Richter, *Rev. Mod. Phys.* **82**, 2365 (2010).
39. J. Birkhan *et al.*, submitted; arXiv:1308.2817 [nucl-ex].
40. A. Shevchenko *et al.*, *Phys. Rev. Lett.* **93**, 122501 (2004).
41. Y. Kalmykov *et al.*, *Phys. Rev. Lett.* **96**, 012502 (2006).
42. Y. Kalmykov *et al.*, *Phys. Rev. Lett.* **99**, 202502 (2007).